Glacial-interglacial changes of continental weathering: Estimates of the related CO_2 and HCO_3^- flux variations and their uncertainties

Guy Munhoven [a,b,*]

[a] *Laboratoire de Physique Atmosphérique et Planétaire*
Institut d'Astrophysique et de Géophysique
Université de Liège
5, avenue de Cointe,
B–4000 Liège

[b] *Bristol Glaciology Centre,*
School of Geographical Sciences,
University of Bristol,
Bristol, BS8 1SS, U.K.

Abstract

A range of estimates for the glacial-interglacial variations in CO_2 consumption and HCO_3^- production rates by continental weathering processes were calculated with two models of continental weathering: GKWM (Gibbs and Kump, 1994) and GEM-CO_2 (Amiotte Suchet and Probst, 1993, 1995b). Both models link CO_2 consumption and HCO_3^- production rates to the global distributions of lithology and runoff. A spectrum of thirty-two estimates for the runoff distribution at the Last Glacial Maximum (LGM) was constructed on the basis of two different data sets for present-day runoff and climate results from eight GCM climate simulation experiments carried out in the framework of the Paleo Modelling Intercomparison Project (PMIP). With these forcings, GKWM produced 3.55–9.0 Tmol/yr higher and GEM-CO_2 4.7–13.25 Tmol/yr higher global HCO_3^- production rates at the LGM. Mean variations (plus/minus one standard error of the mean with seven degrees of freedom) were 6.2 ± 0.6 Tmol/yr and 9.4 ± 1.0 Tmol/yr respectively. The global CO_2 consumption rates obtained with GKWM were 1.05–4.5 Tmol/yr (mean: 2.8 ± 0.4 Tmol/yr) higher at the LGM than at present. With GEM-CO_2, this increase was 1.95–7.15 Tmol/yr (mean: 4.8 ± 0.6 Tmol/yr). The large variability in the changes obtained with each weathering model was primarily due to the variability in the GCM results.

The increase in the CO_2 consumption rate due to continental shelf exposure at the LGM was always more than 60% larger than its reduction due to ice cover. For HCO_3^- production rates, the increase related to shelf exposure was always more than twice as large as the decrease due to ice cover. Flux variations in the areas exposed both now and at the LGM were, in absolute value, always more than 3.5 times lower than those in the shelf environment.

The calculated CO_2 consumption rates by carbonate weathering were consistently higher at the LGM, by 2.45–4.5 Tmol/yr (mean: 3.4 ± 0.2 Tmol/yr) according to GKWM and by

2.75–6.25 Tmol/yr (mean: 4.6 ± 0.4 Tmol/yr) according to GEM-CO_2. For silicate weathering, GKWM produced variations ranging between a 1.9 Tmol/yr decrease and a 0.4 Tmol/yr increase for the LGM (mean variation: -0.7 ± 0.2 Tmol/yr); GEM-CO_2 produced variations ranging between a 0.8 Tmol/yr decrease and a 1.05 Tmol/yr increase (mean variation: $+0.2 \pm 0.2$ Tmol/yr). In the mean, the calculated variations of CO_2 and HCO_3^- fluxes would contribute to reduce atmospheric p_{CO_2} by 5.7 ± 1.3 ppmv (GKWM) or 12.1 ± 1.7 ppmv (GEM-CO_2) which might thus represent a non negligible part of the observed glacial-interglacial variation of ~ 75 ppmv.

Key words: carbon dioxide, chemical weathering, runoff, last glacial maximum, numerical models

1 Introduction

The abundance of CO_2 in the atmosphere was only 190–200 ppmv at the Last Glacial Maximum (LGM, about 21,000 years ago), compared to 260–280 ppmv during the Holocene, as documented by polar ice core records (Delmas et al., 1980; Neftel et al., 1982; Barnola et al., 1987). These oscillations between similar low glacial and high interglacial values were confirmed for the past 420,000 years (Jouzel et al., 1993; Petit et al., 1999). It was recognised very early (Broecker, 1982) that the ocean plays the major role for controlling atmospheric CO_2 levels over glacial-to-interglacial time scales.

Riverine inputs of dissolved inorganic carbon and alkalinity produced by continental weathering play an important role for the long-term evolution of the oceanic carbon cycle. On time scales of a few thousands of years, these two inputs control the total accumulation of marine biogenic carbonate on the sea-floor (Broecker and Peng, 1987). Carbonate accumulation is, however, also closely linked to the carbonate ion concentration in the deep sea (Broecker and Peng, 1982). Via seawater carbonate chemistry, continental weathering processes may thus influence atmospheric CO_2 levels over the time scales of the glacial-interglacial transitions.

Present-day rates of CO_2 consumption by carbonate and silicate weathering are each about 12×10^{12} mol CO_2/yr (Meybeck, 1987; Gaillardet et al., 1999). Based on the carbon cycle model of Munhoven and François (1996), it can be estimated that a 1×10^{12} mol CO_2/yr increase in the annual CO_2 consumption by carbonate weathering at the LGM relative to the present day would lead to a net 2.4 ppmv decrease of atmospheric p_{CO_2} (and vice versa), all oceanic and sedimentary feedbacks being taken into account. For a similar increase in silicate weathering, atmo-

* Currently at Laboratoire de Physique Atmosphérique et Planétaire, Université de Liège. *Email address:* `Guy.Munhoven@ulg.ac.be` (Guy Munhoven).

spheric p_{CO_2} would decrease by 4.1 ppmv. Variations of up to 20% of the two rates could hence be responsible for net p_{CO_2} changes of 15 ppmv, either contributing to or counteracting the observed variations. A full understanding of the observed $\sim$ 75 ppmv oscillation will clearly require a precise reconstruction of continental weathering fluxes over that time scale. Currently available reconstructions for CO_2 consumption or HCO_3^- production rates at the LGM give, however, very contrasting results.

The surface of the Earth was cooler at the LGM. Extensive ice-sheets covered large parts of the continents at high latitude. Kump and Alley (1994) point out that chemical weathering rates should have been largely reduced under these circumstances. On the other hand, the global sea level stood 120–130 m lower (Chappell and Shackleton, 1986; Fairbanks, 1989). As a consequence, large extents of the currently flooded continental shelf lay free and were subject to erosion. Gibbs and Kump (1994) were the first to produce a quantitative estimate for the effect that these large-scale changes had on global chemical weathering. They use a model of continental weathering linking bicarbonate production rates to the spatial distributions of exposed rock types and runoff. They find that the total bicarbonate production rate was about 20% higher at the LGM than today. An additional 80% increase could come from ice-marginal areas if chemical weathering was proceeding there at a high rate.

Munhoven and François (1996) use the marine Ge/Si record (Froelich et al., 1992) to calculate that silicate rock weathering processes alone fixed 100–250% more CO_2 at the LGM than at present. Such an increase in CO_2 consumption would contribute a 30–90% increase in total HCO_3^- production. Recent findings on the marine Ge and Si cycles indicate that Si fluxes related to dust dissolution in the surface ocean (Kurtz and Derry, 1998) or to early diagenesis (Hammond et al., 2000; King et al., 2000) might play important roles in driving the marine Ge/Si ratio on glacial-interglacial time scales. Including these processes in the calculations of Munhoven and François (1996) might lead to significantly different results.

Ludwig et al. (1999) adopt a similar approach to Gibbs and Kump (1994), using the "Global Erosion Model for CO_2 Consumption" (GEM-CO_2, Amiotte Suchet and Probst, 1995b) to propose two different estimates of glacial-interglacial variations of continental weathering CO_2 consumption rates. Unlike Gibbs and Kump (1994), Ludwig et al. (1999) do not perform a full reconstruction of the continental shelf environment. For their first estimate, Ludwig et al. (1999) derive the LGM shelf weathering fluxes by extrapolation from the present-day land area which was exposed at the LGM. They find that the total CO_2 consumption rate was about 5% lower at the LGM than at present. CO_2 consumption by silicate weathering was 1% lower. Hence HCO_3^- production was 7% lower. Their second estimate is based on a series of sensitivity tests regarding the influence of the exposed rock types on the shelf at the LGM. For a shelf lithology broadly similar to that of Gibbs and Kump (1994), Ludwig et al. (1999) expect that the total consumption of CO_2 would have

been 20% higher at the LGM than in the present day, with a 10% lower CO_2 consumption by silicate weathering. Accordingly, the total HCO_3^- production would have been 33% higher at the LGM.

However, there are substantial differences between the two weathering models used by Gibbs and Kump (1994) and Ludwig et al. (1999). The two studies are also based on different geographical and climatic boundary conditions. It is not clear to what extent the differences between the results produced by Gibbs and Kump (1994) and Ludwig et al. (1999) reflect uncertainties arising from poorly constrained climate forcings (e. g. runoff distribution), and to what extent they reflect instrinsic model differences.

A first aim of this study was therefore to perform a quantitative intercomparison of the two weathering models. Both were adapted as far as possible in order to bring them in line with each other. Each of the two weathering models was then applied with two different data sets depicting the present-day runoff distribution.

A second aim of the study was the exploration of the spectrum of possible variations of CO_2 consumption and HCO_3^- production over glacial-interglacial time scales. This was made possible by the existence of a number of different publicly available data sets from GCM climate simulation experiments for the LGM, carried out within the framework of the Paleo Modelling Intercomparison Project (PMIP, Joussaume and Taylor, 1995, 2000). By combining the two distributions for present-day runoff with the precipitation-minus-evaporation ($P - E$) distributions from eight selected GCM data sets, sixteen different estimates for the distribution of glacial-to-interglacial runoff variations could be constructed for use with both weathering models. Furthermore, a common configuration of the shelf exposed at the LGM was developed for use with both models, based on the topographical reconstructions of Peltier (1994) and the shelf lithology provided by Gibbs and Kump (1994).

Finally, the model results were analysed in order to determine the respective contributions from the three large-scale environmental changes that affected the Earth surface at the LGM: (1) flux reduction due to ice cover, (2) flux increase from shelf exposure, and (3) variations in the land exposed both now and at the LGM. Neither Gibbs and Kump (1994) nor Ludwig et al. (1999) provide a complete analysis of their results in terms of individual contributions from these three large-scale environmental changes. Gibbs and Kump (1994) only present total HCO_3^- fluxes for the present day and the LGM. Ludwig et al. (1999) report total CO_2 and silicate weathering CO_2 consumption rates for the LGM. They also break down the two fluxes into contributions from present-day land and from the exposed shelf. However, it is unknown how much of the flux variations over present-day land calculated by Ludwig et al. (1999) is due to the extended ice cover and to runoff variations over areas exposed both now and at the LGM.

Preliminary results of this study were published in Munhoven (1999), together with additional sensitivity tests regarding shelf lithology (not reported here). That study was based on versions of the two weathering models which included the original incompatible continental outlines and two different shelf reconstructions. Calculations could also be based only on a few already dated GCM simulation experiments. Furthermore, no correction was made in that study to resolve inconsistencies arising from incompatibilities between the weathering model and the climate model land masks. All these problems are addressed in the present study.

2 Methodology: Model and data description

This section gives a short presentation and discussion of the two weathering models under consideration. The procedures adopted to perform the calculations with the two models are detailed, and the adaptations that were applied in order to make them compatible are presented. Finally, it is explained how the various boundary conditions and climate forcings required for their application under LGM climate conditions were defined.

2.1 The weathering models: GKWM and GEM-CO_2

The rationale behind the two weathering models is essentially the same. Both models are based on a map of global lithology. Distributions of CO_2 consumed and HCO_3^- produced by chemical weathering are linked to the distribution of runoff intensity, using a set of empirical bicarbonate flux-runoff relationships for major rock types. In both models, weathering rates beneath ice are neglected.

The Gibbs and Kump (1994) weathering model (hereafter GKWM) is based on a $2^\circ \times 2^\circ$ map of global lithology. Six classes of rock types are distinguished: carbonates, shales, sandstones, extrusive igneous rocks, shields and a complex class, for grid points not clearly fitting into any of the first five classes. The $1^\circ \times 1^\circ$ map used with GEM-CO_2 differentiates between seven classes (Amiotte Suchet and Probst, 1995b): carbonates, shales, sands and sandstones, plutonic and metamorphic rocks, acid volcanic rocks, basalts, and evaporites. The empirical bicarbonate flux-runoff relationships used in GKWM are taken from Bluth and Kump (1994). These were calculated from chemical analyses of stream water from a large number essentially monolithologic watersheds, underlain by carbonates, shales, sandstones, basalt and granite. The relationships used with GEM-CO_2 are derived from Meybeck's (1986) chemical analyses of stream water from small monolithologic and essentially non-polluted watersheds in France (Amiotte Suchet and Probst, 1993).

Amiotte Suchet and Probst (1995b) formulate GEM-CO_2 in terms of CO_2 con-

sumed, assuming that for all rock types, except for carbonates and evaporites, all of the HCO_3^- in the stream water comes from the atmosphere. Streams draining carbonate and evaporite rocks are assumed to follow carbonate dissolution stoichiometry, i. e., one half of the HCO_3^- in the stream water is supposed to come from the atmosphere and the other half from the dissolving rock minerals. Gibbs and Kump (1994) on the other hand focus on HCO_3^- production only in GKWM. For the purpose of this study, GKWM was extended to provide CO_2 consumption rates as well. The same rationale as in GEM-CO_2 was followed: HCO_3^- in water draining carbonate rocks was supposed to be made up for one half of CO_2 coming from the atmosphere and for one half of CO_3^{2-} ions coming from the dissolving (carbonate) minerals. In waters draining other rock types than carbonates, all HCO_3^- was assumed to come from the atmosphere. This assumption is clearly a simplification, and it was already recognized as such by Amiotte Suchet and Probst (1995b) who emphasize that especially shales and sandstones are rarely completely devoid of carbonate minerals. Besides this, it has also be shown that disseminated calcite plays a role in the chemical weathering of granitoid rocks (White et al., 1999). However, it is essential to know about both HCO_3^- production *and* CO_2 consumption rates if sensible quantitative conclusions regarding the impact of changing continental weathering processes in the evolution of atmospheric CO_2 on glacial-interglacial time scales are to be drawn. It must therefore be kept in mind that the estimates for the latter as calculated by the type of weathering model used here are likely to be overestimates.

The two sets of relationships giving the specific CO_2 consumption rates as a function of runoff used with the two models are compared in Figure 1.

It appears that, for any given type of rock exposure, there can be large differences between the CO_2 consumption rates (and equivalently HCO_3^- production rates) predicted by the two models. At runoff values close to the continental average (about 412 mm/yr over areas draining to the oceans according to the two runoff data sets used in this study), GEM-CO_2 predicts either similar or considerably lower rates than GKWM. GEM-CO_2 rates are lower by a factor of 3.5 in the case of plutonic and metamorphic rocks, and 1.8 in the case of shales. For carbonate outcrops on the other hand, GEM-CO_2 rates are always higher than GKWM ones: 22% at 412 mm/yr, and 30% at 1000 mm/yr. As a consequence it should be expected that the global HCO_3^- flux derived from GKWM is characterised by a much smaller crustal contribution (and accordingly, a lower atmospheric contribution) than that calculated with GEM-CO_2, assuming that the two models use broadly similar lithology maps.

Amiotte Suchet and Probst (1995b) have only published maps of the present-day distributions of the annual CO_2 consumption and HCO_3^- production rates and made them available to the public (Amiotte Suchet and Probst, 1995a). These two maps contain all the information that is necessary to carry out the calculations with GEM-CO_2 (with a negligibly small loss of accuracy). The empirical CO_2 flux-runoff rela-

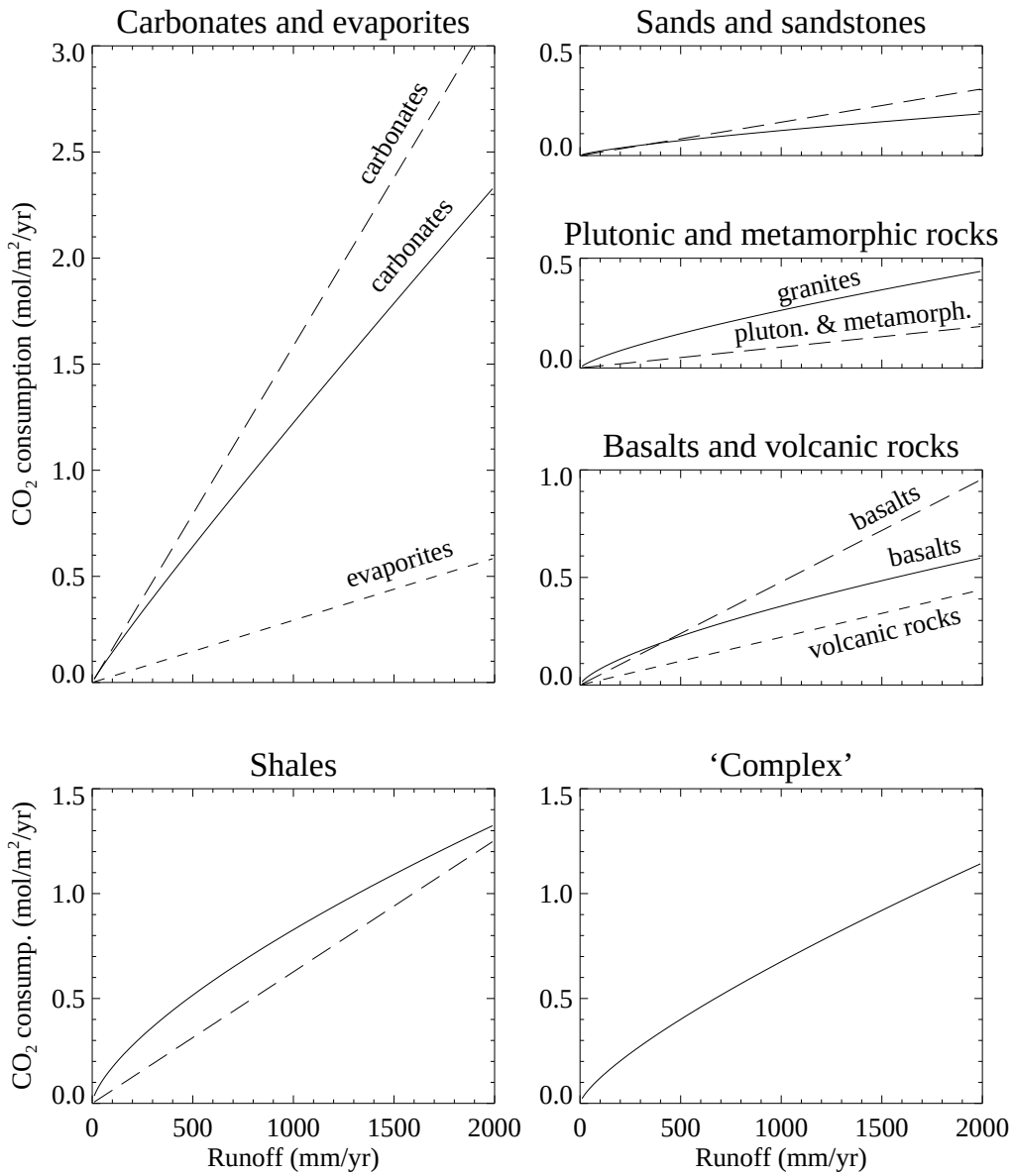

Fig. 1. CO_2 flux-runoff relationships used in GKWM (solid lines, after Bluth and Kump (1994)) and GEM-CO_2 (dashed lines, after Amiotte Suchet and Probst (1993, 1995a)). There is no 'complex' class for GEM-CO_2.

tionships used in GEM-CO_2 are linear. Hence, two CO_2 consumption rate distributions F and F_0 obtained from GEM-CO_2 from two runoff distributions R and R_0 are related by $F/F_0 = R/R_0$. The CO_2 flux distribution (F_0) that Amiotte Suchet and Probst (1995a,b) calculated from a runoff distribution (R_0) which they derive from the monthly precipitation and evapotranspiration data of Willmott et al. (1985) can therefore be used to calculate the CO_2 flux distribution (F) produced by GEM-CO_2 for an arbitrary runoff distribution (R) by setting $F = R \times (F_0/R_0)$. The ratio (F_0/R_0) is, at each grid point, equal to the constant factor of the empirical CO_2 flux-runoff relationship that characterizes the underlying lithological class. HCO_3^-

production rates are obtained in a similar way. At grid points where R_0 is equal to zero, F is also set to zero. This simplification does not significantly affect the global flux estimates calculated here. The grid points at issue represent only 2.8% of the externally drained area (101.7 millions of km^2). In the GGHYDRO runoff distribution (see below), e. g., they account for less than 0.2% of the total external runoff from ice-free areas (44,700 km^3/yr). Because of the linear formulation of GEM-CO_2 it can be expected that the differences on the CO_2 and HCO_3^- fluxes due to this approximation are also of the order of a few tenths of a percent at most.

The components necessary to perform calculations with GKWM directly have been fully published (Gibbs and Kump, 1994; Bluth and Kump, 1994). Following Gibbs and Kump (1994), the 'complex' lithology class was assigned a globally constant composition in terms of the five basic rock types considered and an accordingly weighted average of the five basic flux-runoff relationships was used. The composition used here is from Jones et al. (1999). It was calculated in such a way that the global areal distribution of the five basic rock types in the GKWM lithology map would match that of the map in GEM-CO_2 (Amiotte Suchet, 1995, Table 12). Finally, it should be mentioned that, before use, the GKWM lithology map was regridded onto the same $1^\circ \times 1^\circ$ grid as GEM-CO_2. A simple redistribution procedure was used for this purpose.

2.2 Present-day geography: ice cover and continent outlines

No information regarding present-day ice cover can be retrieved from the CO_2 and HCO_3^- flux maps provided by Amiotte Suchet and Probst (1995a). The ice distribution from the GGHYDRO data base (Cogley, 1998) was therefore used with GEM-CO_2 for the present day. The GGHYDRO data base was furthermore used to complete the continental outlines for GEM-CO_2, as Antarctica and Greenland were not considered in the study of Amiotte Suchet and Probst (1995a). Gibbs and Kump (1994) provide continental outlines with their lithological map, for both present-day and LGM conditions. In the course of the shelf reconstruction procedure, they were adjusted in order to improve the compatibility between the two models' masks for both present-day and LGM continents.

2.3 LGM geography: ice cover, shelf extent and shelf lithology

The ice-sheet extent from Peltier (1994) was used with both models and was not modified. The boundaries of the exposed shelf were reconstructed from the topographical reconstructions of Peltier (1994). There are substantial differences between the continental outlines derived from the weathering model maps and from Peltier's (1994) present-day topographical map. The high-resolution elevation data

base ETOPO5 (ETOPO5, 1988) was therefore considered to produce an independent reference mask. The data from ETOPO5 were first down-gridded from their $5' \times 5'$ grid to a $1° \times 1°$ grid. Land areas were defined by all the grid elements with positive elevations. Among the four maps, the best agreement was found between the GEM-CO_2 continental outlines and the $1° \times 1°$ version of ETOPO5. Peltier's (1994) maps were therefore only used to calculate the distribution of glacial-interglacial topography anomalies. The actual LGM topography was obtained by adding the anomalies onto the ETOPO5-derived map. The LGM ocean was then defined to consist of all grid elements with negative elevations that were not covered by ice. The rest was supposed to make up the LGM land (unflooded shelf included).

The extent of shelf exposed at the LGM was defined to consist of all the grid elements belonging to the present-day ocean in the GEM-CO_2 land mask on one hand, and lying within the LGM land limits on the other hand. Chosing the GEM-CO_2 land mask as a reference here instead of the ETOPO5 avoids further adjustments to be made for its use, and does not lead to any significant differences. This shelf exposure was used with both weathering models. The GKWM continental outlines were then adjusted, supposing that the present-day continent is made up by all the grid-elements in Gibbs and Kump's (1994) original map that are neither part of the ocean nor of the newly delimited exposed shelf. For both GEM-CO_2 and GKWM, the lithology of the exposed shelf was taken from Gibbs and Kump's (1994) map wherever possible. Remaining points (covered by ocean in the GKWM, and which represent 25% of the exposed shelf area here) were assigned a constant mixed lithology. The mixture was chosen so as to obtain the same global average shelf lithology as in the original GKWM (Gibbs and Kump, 1994). In the original GKWM, the shelf exposed at the LGM is covered by carbonates, shales and sandstones in areal proportions of 45%, 40% and 15% respectively. There were no extrusive igneous or shield rocks in the shelf configuration of Gibbs and Kump (1994). Grid points of these two classes that got remapped onto the exposed shelf as a result of the continental boundary adaptations were therefore also converted to the mixed lithology class. To reach the average composition above, a mixture of 65% carbonates, 27.5% shales and 7.5% sandstones had to be adopted for these points of unidentified lithology. A series of sensitivity tests were carried out where the composition of the mixture was refined and calculated as a function of latitude by a least squares procedure, so that the areal proportions of the three rock types represented on the shelf would fit those of the original GKWM not only at the global scale, but also in zonal bands of various widths.

In order to compare the effects of the increased ice-coverage and the extended shelf exposure, and to assess the total variations of the bicarbonate production and CO_2 consumption rates between the LGM and the present day, the following partitioning of the LGM continental area into five non-overlapping classes is considered.

- L1: presently exposed land that was also exposed at the LGM;

Table 1
Surface areas for the different zones.

Land mask	L1[a]	L2[a]	L3[a]	S1[a]	S2[a]	L1+L2	L1+S1
Total continent							
GKWM (Gibbs and Kump, 1994)	114.0	—	—	15.9[b]	—	133.2	129.9
GKWM (this study)	114.1	17.8	15.9	13.2	11.8	131.9	127.3
GEM-CO_2 (this study)	116.2	17.2	15.7	13.2	12.8	133.4	129.4
GEM-CO_2 (Ludwig et al., 1999)	118.0	19.2	15.3	12.3	8.1	137.2	130.3
Externally drained							
GKWM (Gibbs and Kump, 1994)	89.2	—	—	15.9[b]	—	108.2	105.1
GKWM (this study)	82.8	17.2	15.9	13.2	11.8	100.0	96.0
GEM-CO_2 (this study)	84.8	16.9	15.7	13.2	12.8	101.7	98.0
GEM-CO_2 (Ludwig et al., 1999)	87.2	19.1	15.3	12.3	8.1	106.3	99.5

All surface areas are given in 10^6 km^2. Surface areas for the model configurations used in Gibbs and Kump (1994) and Ludwig et al. (1999) were recalculated from the original reported figures. Entries marked '—' could not be unambiguously determined.
[a] L1 – land exposed now and at the LGM; L2 – land exposed now and covered by ice at the LGM; L3 – land covered by ice now and at the LGM; S1 – shelf flooded now and exposed at the LGM; S2 – shelf flooded now and covered by ice at the LGM; L1+L2 – total area exposed now; L1+S1 – total area exposed at the LGM.
[b] 12.3×10^6 km^2 as directly calculated from the map published by Gibbs and Kump (1994). Accordingly, the surface areas of L1 become 117.6×10^6 km^2 (total continent) and 92.8×10^6 km^2 (externally drained).

- L2: presently exposed land that was covered by ice at the LGM;
- L3: presently ice-covered land that was also covered by ice at the LGM;
- S1: presently flooded shelf that was exposed at the LGM;
- S2: presently flooded shelf that was covered by ice at the LGM.

Over zone L1, runoff variations can lead to increases or decreases of the CO_2 and HCO_3^- fluxes. All over zone L2, the presence of ice reduced the weathering fluxes to zero at the LGM, thus invariably contributing to a decrease of both CO_2 and HCO_3^- fluxes. Zone S1 invariably contributes to a global increase of both CO_2 and HCO_3^- fluxes. Zones L3 and S2 do not have any impact on the glacial-interglacial variations of continental weathering fluxes. The surface areas covered by the five zones in the two models are reported in Table 1. The drainage pattern used to distinguish between internally and externally drained areas was taken from Cogley (1998). The surface areas of the corresponding regions from the studies of Gibbs and Kump (1994) and Ludwig et al. (1999) are given for comparison, as far as it was possible to derive them from the original studies. Differences between the two adapted models used here, and their respective original versions are due to the dif-

ferent ice-sheet reconstructions used and the different reconstructions for the shelf exposure. Regarding GEM-CO_2, it should be noticed that the presently exposed land areas around the border of Greenland and in Antarctica are not represented here, whereas they are in the study of Ludwig et al. (1999). In Table 1, they are included with the ice-covered emerged shelf (S2) for the GEM-CO_2 version used here, and with the present-day exposed land that got covered by ice at the LGM (L2) in the version of Ludwig et al. (1999). Small discrepancies between the GEM-CO_2 and GKWM versions used here can be explained by remaining differences between the continental outlines of the two models, basically resulting from different inital grid resolutions.

2.4 Runoff: present-day distributions and reconstructions for the LGM

Gibbs and Kump (1994) base their study on a numerical version of the runoff maps from the UNESCO Atlas of World Water Balance (Korzoun et al., 1977). Ludwig et al. (1999) use an empirical approach rooted in the precipitation distribution taken from that same UNESCO Atlas and the temperature distributions from Legates and Willmott (1990). Amiotte Suchet and Probst (1995a,b) derive their runoff distribution from the monthly mean precipitation (P) and evapotranspiration (E) data sets of Willmott et al. (1985), identifying annual runoff and the sum of positive monthly $P-E$ differences over a year.

In this study, two different data sets for the present-day distribution of continental runoff were considered :

- GGHYDRO: runoff distribution from the hydrographic database GGHYDRO (Cogley, 1998). This runoff distribution largely derives from the UNESCO data.
- UNH-GRDC: composite runoff fields obtained by assimilating river discharge data into a climate-driven water balance model (Fekete et al., 2000).

Calling upon two such data sets helps to gain insight into the basic variability of the global fluxes derived from the two models, only due to uncertainties in the present-day runoff distribution. GGHYDRO and UNH-GRDC draw slightly different pictures of the global drainage distribution at the Earth surface (Table 2). The most important differences occur at high latitudes, as illustrated by the significantly different drainage volumes from zone L2. The small differences between the global drainage volumes calculated from the two land masks are due to remaining differences between the respective continental outlines.

It can be expected that GGHYDRO comes close to the runoff distribution used by Gibbs and Kump (1994). The runoff distribution used by Amiotte Suchet and Probst (1995a,b) was not considered for this study. The monthly mean $P-E$ differences calculated from Willmott et al.'s (1985) P and E data add up to an annual total volume from externally drained areas of 32,100 km^3 only. This volume is un-

Table 2
Present-day drainage volumes for ice-free areas.

Data set	Zone	GKWM land mask Total continent	GKWM land mask Externally drained	GEM-CO_2 land mask Total continent	GEM-CO_2 land mask Externally drained
GGHYDRO	L1	37,300	35,900	38,400	37,000
	L2	8,300	7,900	7,800	7,700
	L1+L2	45,600	43,800	46,200	44,700
UNH-GRDC	L1	33,400	32,200	34,600	33,300
	L2	6,200	5,900	5,800	5,700
	L1+L2	39,600	38,100	40,400	39,000
Average	L1	35,400	34,100	36,500	35,200
	L2	7,200	6,900	6,800	6,700
	L1+L2	42,600	41,000	43,300	41,900

All figures are given in km^3, i.e., 10^9 m^3/yr, and were rounded to the nearest hundred before reporting.

realistically low, in comparison with the volumes derived from GGHYDRO and UNH-GRDC, which are both based on river gauging data (cf. Table 2). The positive monthly $P-E$ differences add up to an annual volume of 41,300 km^3 from externally drained areas, in good agreement with observational values. However, adding up the positive monthly differences only would be at odds with the mass balance principles at the basis of the calculations of Willmott et al. (1985).

Similar to Gibbs and Kump (1994) and Ludwig et al. (1999) (and also Munhoven (1997, 1999)) the reconstructions of the LGM runoff distribution that could be used as inputs for GKWM and GEM-CO_2 were derived from climate simulation experiment results carried out with atmospheric General Circulation Models (GCMs). For this study GCM results from the Paleoclimate Modelling Intercomparison Project (PMIP, Joussaume and Taylor, 1995, 2000) were used.

In the framework of PMIP, climate simulations experiments were carried out for the mid Holocene (6 kyr B.P.) and the LGM (21 kyr B.P.), together with appropriate control runs for the present day. The participating modelling groups adopted standardized boundary conditions for all runs (Joussaume and Taylor, 1995, 2000). All of the LGM experiments used Peltier's (1994) reconstructions of ice-sheet heights and extents, which were also used for this study. Atmospheric CO_2 levels were set to 200 ppmv, in accordance with ice-core records (e. g., Barnola et al., 1987; Jouzel et al., 1993). Earth's orbital parameters were modified to reflect those 21 kyr B.P. As there remain substantial uncertainties regarding sea surface temperature (SST) reconstructions for the LGM, two different types of experiments were defined (see

Joussaume and Taylor, 1995, 2000). The first type uses a prescribed distribution of SSTs derived from the CLIMAP reconstruction (CLIMAP Project Members, 1981); for the second type it is assumed that the ocean heat transport remained constant and SSTs are computed accordingly with a coupled model of the surface ocean. For this study, eight different output data sets were selected from the most recent version of the PMIP data base (version R03-2001d). The eight selected data sets include four experiments of each type. The adopted selection criteria are detailed below.

As no explicit runoff distributions were provided in the PMIP data base, the difference between the total annual precipitation and evaporation, $P-E$, was used as a proxy for annual continental runoff with the eight GCMs. In a steady-state regime, the annual $P-E$ matches annual runoff.

Runoff values, R_{LGM}, for grid elements falling on land at the LGM were estimated by setting

$$\begin{cases} R_{\mathrm{LGM}} = R_{\mathrm{obs}} + \Delta R, \\ R_{\mathrm{LGM}} \geq 0. \end{cases} \tag{1}$$

In this equation R_{obs} is the present observed value, taken from either GGHYDRO or UNH-GRDC. ΔR is the anomaly relative to the present, calculated from the GCM climatologies:

$$\Delta R = (P-E)_{\mathrm{GCM(LGM)}} - (P-E)_{\mathrm{GCM(present)}}. \tag{2}$$

The subscripts ‘GCM(LGM)’ and ‘GCM(present)’ refer to GCM results from the LGM and the present-day (control) experiments respectively. A lower bound of 0 mm/yr was imposed on R_{LGM} values to avoid physically meaningless negative values. The combination of the two runoff with the eight GCM data sets provided sixteen different estimates for the LGM runoff distribution that could be used with the two weathering models.

Before equation (1) could be applied to the whole exposed LGM land area, the observed present-day runoff distributions had to be extrapolated onto the currently flooded shelf that was exposed at the LGM. The GCM results were regridded onto the $1^\circ \times 1^\circ$ grid of the weathering models, using an area-weighted remapping scheme. In order to derive sensible results from equation (2) on the $1^\circ \times 1^\circ$ grid, one additional adaptation had to be performed. Continental outlines on the various GCM grids and on the weathering models’ $1^\circ \times 1^\circ$ grids are incompatible. Hence, a straight remapping of the GCM $P-E$ distributions may lead to $P-E$ values from the GCM’s *oceanic* grid elements being inadvertently mapped onto *continental* elements in the weathering model grids. As $P-E$ is generally negative over the oceans, the use of such oceanic values in equation (1) would lead

Table 3
List of GCM output datasets and global annual $P-E$ over externally drained areas, with and without correction (see text for details).

Model experiment	Ref.	GKWM land mask		GEM-CO_2 land mask	
		Straight interpolation	Corrected interpolation	Straight interpolation	Corrected interpolation
BMRC2.fix	(1)	31,200	31,200	31,400	31,600
CCC2.0.fix	(2)	27,400	34,500	26,900	35,300
ECHAM3.fix	(3)	37,300	40,300	37,600	41,200
LMCELMD5.fix	(4)	57,100	50,500	57,600	53,400
CCC2.0.cal	(2)	26,100	33,700	25,400	34,600
CCM1.cal	(5)	36,400	42,200	36,100	43,000
GFDL.cal	(6)	49,200	52,700	49,200	53,600
UKMO.cal	(7)	28,200	31,500	28,000	32,000

References (to experiment description where available, else to model description): (1) Colman and McAvaney (1995); (2) McFarlane et al. (1992); (3) Lorenz et al. (1996); (4) Masson et al. (1998); (5) Kutzbach et al. (1998); (6) Broccoli and Manabe (1992); (7) Hewitt and Mitchell (1997).

to erroneous, if not physically meaningless, runoff values. To avoid this problem, the $P-E$ distributions obtained from each GCM were therefore extrapolated from the GCM's continental grid elements onto its oceanic ones *before* regridding them. $P-E$ values over continental elements on the GCM grid were left unchanged.

In consequence, only data produced by such GCMs that allowed an unequivocal characterization of their grid elements as either oceanic or continental (i. e., no fractional land/ocean cover at any given grid element) could be considered. As an additional quality index, it was required that the so adapted GCM $P-E$ distributions would, after interpolation onto the $1^\circ \times 1^\circ$ grid, yield a global annual water flux from externally drained areas falling within $\pm 30\%$ of the average observed annual runoff volume as documented by the two adopted runoff datasets GGHYDRO and UNH-GRDC (see Table 2).

The eight GCM data sets that fulfilled these criteria are listed by their acronyms in Table 3: '.fix' suffixes refer to simulation experiments carried out with prescribed (fixed) SSTs; '.cal' suffixes refer to those with calculated SSTs. Summary descriptions and complete literature references for all of the models participating in PMIP can be found on the PMIP WWW site (http://www-pcmdi.lln.gov/pmip). Also reported in Table 3 are the total annual $P-E$ volumes over the presently ice-free and externally drained continental area as calculated from the regridded GCM $P-E$ distributions, without and with application of the land-to-ocean extrapola-

tion described above, for both GKWM and GEM-CO_2 landmasks. The impact of the corrective extrapolation before regridding is obvious. Except for BMRC2.fix (where the corrected and uncorrected figures are virtually identical) and for LM-CELMD5.fix (where the corrected figures are about 10% lower than the uncorrected ones), the total integrated volume of the regridded $P-E$ distribution became between 10% and more than 30% higher as a result of the applied correction.

3 Results and discussion

The main focus will be on the fluxes from externally drained areas in this discussion, although results relative to the total continental area are occasionally reported as well. Fluxes from externally drained areas are the more important ones in the global carbon cycle, since they link the terrestrial to the oceanic environment.

The most recent estimates for CO_2 consumption rates by continental silicate and carbonate weathering and the corresponding HCO_3^- production rates are those of Gaillardet et al. (1999). Using an extensive set of hydrochemistry data for sixty of the largest rivers in the World, Gaillardet et al. (1999) calculate that continental silicate weathering processes globally consume 11.7 Tmol CO_2/yr, 8.7 Tmol/yr of which arise from the weathering of continental rocks and 3.0 Tmol/yr from the weathering of volcanic rocks from oceanic islands and volcanic arcs (1 Tmol = 10^{12} mol). Gaillardet et al. (1999) also calculate that carbonate weathering processes consume 12.3 Tmol of CO_2 each year. The total CO_2 consumption rate is thus 24.0 Tmol/yr. Accordingly, the total rate of HCO_3^- production by continental weathering processes is 36.3 Tmol/yr (24.0 Tmol/yr steming from the atmosphere and 12.3 Tmol/yr from the dissolving carbonate minerals). These figures are in good agreement with the earlier estimates of Meybeck (1987). The figures from Gaillardet et al. (1999) will be used as present-day reference values in the following discussion.

3.1 Present-day CO_2 consumption and HCO_3^- production rates

3.1.1 Model results for present-day conditions

In a preliminary assessment exercise, GKWM and GEM-CO_2 were applied directly with the two runoff distribution data sets GGHYDRO and UNH-GRDC as forcings to evaluate their respective performances for present-day conditions. The calculated global HCO_3^- production and CO_2 consumption rates are reported in Table 4, along with values previously obtained with the two models and the estimates from the literature mentioned above.

Table 4
Present-day HCO_3^- production and CO_2 consumption rates by continental weathering: total fluxes and apportionment to silicate and carbonate weathering processes.

		Total continent				Externally drained			
		HCO_3^- total	CO_2 total	CO_2 silic.	CO_2 carb.	HCO_3^- total	CO_2 total	CO_2 silic.	CO_2 carb.
This study	GKWM & GGHYDRO	30.4	24.5	18.6	5.9	28.6	23.0	17.4	5.6
	GKWM & UNH-GRDC	25.9	20.9	15.9	5.0	24.3	19.6	14.9	4.7
	GEM-CO_2 & GGHYDRO	30.8	21.9	13.0	8.9	29.8	21.2	12.6	8.6
	GEM-CO_2 & UNH-GRDC	26.7	19.1	11.5	7.6	25.7	18.4	11.1	7.3
	GKWM* & GGHYDRO[a]	27.5	20.1	12.7	7.4	26.1	19.1	12.1	7.0
	GKWM* & UNH-GRDC[a]	23.2	17.0	10.8	6.2	22.0	16.1	10.2	5.9
	GEM-CO_2* & GGHYDRO[a]	33.8	26.75	19.7	7.05	32.4	25.6	18.8	6.8
	GEM-CO_2* & UNH-GRDC[a]	29.4	23.35	17.3	6.05	28.1	22.3	16.5	5.8
Gibbs and Kump (1994)		29.8	—	—	—	28.3	—	—	—
Amiotte Suchet and Probst (1995b)[b]		30.9	21.35	11.8	9.55	—	—	—	—
Ludwig et al. (1999)[c]		—	—	—	—	26.7	19.2	11.7	7.5
Meybeck (1987, Table 8)		39.2	26.4	13.7	12.7	36.6	24.6	12.6	12.0
Gaillardet et al. (1999)		—	—	—	—	36.3	24.0	11.7	12.3

All fluxes are given in 10^{12} mol/yr and were rounded before reporting.
[a] See text for details regarding GKWM* and GEM-CO_2*.
[b] Calculated directly from the distributions of Amiotte Suchet and Probst (1995a).
[c] Converted to 10^{12} mol/yr from the authors' figures in Gt C/yr.

Both GKWM and GEM-CO_2 yield HCO_3^- and CO_2 fluxes that are much lower than the adopted reference values from Gaillardet et al. (1999). Concerning CO_2 consumption, GKWM falls short by 4% or 18%, depending on whether GGHYDRO or UNH-GRDC is used as a runoff distribution. GEM-CO_2 falls short by 12% resp. 23%. The global HCO_3^- production rates produced by both models with GGHYDRO are about 20% lower than the reference value from Gaillardet et al. (1999). With UNH-GRDC they are about 30% lower, reflecting the lower global runoff volume of this data set.

Regarding the inter-model variability, it is observed that GKWM yields 4–5% lower total HCO_3^- fluxes than GEM-CO_2 and 7–8% higher CO_2 consumption rates with each of the two runoff distribution data sets. However, the calculated fluxes cover a large range and the difference between the HCO_3^- fluxes derived from GKWM and GEM-CO_2 is barely significant (see Table 4). The same holds for CO_2 consumption rates. As expected, atmospheric CO_2 thus indeed represents a larger part in the HCO_3^- flux obtained with GKWM than with GEM-CO_2. The GKWM fluxes reported in Table 4 indicate that atmospheric CO_2 represents 80–81% of the total HCO_3^-. With GEM-CO_2, this fraction is only 71–72%, much closer to the fractions of 67% and 66% calculated from the fluxes of Meybeck (1987) and Gaillardet et al. (1999) respectively.

Table 4 also provides the partitioning of the CO_2 consumption into parts fixed by silicate and carbonate weathering processes respectively. There are substantial differences between the respective results of the two models. GKWM produces 34–38% higher silicate and 35–36% lower carbonate weathering CO_2 consumption rates than GKWM. Compared to the independent estimates from the literature, good agreement is only observed for GEM-CO_2's silicate weathering CO_2 consumption flux. For carbonate weathering, this same model yields values that are 30 or 40% too low, depending on the runoff distribution used. CO_2 consumption rates obtained from GKWM are about 30 or 50% higher for silicate weathering than the reference values from Gaillardet et al. (1999). For carbonate weathering they are more than 50% lower than the literature estimates.

3.1.2 Assessment of model-model differences

Discrepancies between the global fluxes calculated with GKWM and GEM-CO_2 can only be related to the empirical bicarbonate flux-runoff relationships or to the lithology maps. To obtain a quantitative estimation for the respective impacts of these two factors, two hybrid models were built: (1) GKWM*, based on the lithological map from GKWM and the empirical CO_2 flux-runoff relationships from GEM-CO_2, and similarly (2) GEM-CO_2*, based on the lithology distribution from the GEM-CO_2 version used here and the empirical bicarbonate flux-runoff relationships from GKWM.

The total CO_2 consumption and HCO_3^- production rates, and the silicate and carbonate weathering CO_2 consumption rates obtained with GKWM* and GEM-CO_2* are reported in Table 4 along with the GKWM and GEM-CO_2 results already discussed. Changing the empirical relationships in a given model leads globally to the most important differences in the calculated fluxes. For any given lithology distribution, switching from GEM-CO_2 to GKWM relationships makes the total HCO_3^- production rate increase by 9–11%, total CO_2 consumption rate by 20–22%, and the silicate weathering CO_2 consumption by as much as 44–49%, and it makes carbonate weathering CO_2 consumption decrease by 20–21%, as documented by the GKWM÷GKWM* and GEM-CO_2*÷GEM-CO_2 ratios of these four fluxes. With any given set of empirical bicarbonate flux-runoff relationships, switching from the GEM-CO_2 to the GKWM lithology distribution leads to less important and more evenly distributed changes, as documented by the GKWM÷GEM-CO_2* and GKWM*÷GEM-CO_2 flux ratios: the total HCO_3^- production decreases by 12–14%, the total CO_2 consumption by 10–12%, silicate weathering CO_2 consumption by 4–10%, and carbonate weathering CO_2 consumption by 18–19%.

The largest part of the differences between GKWM and GEM-CO_2 results appears thus to be related to their different sets of empirical bicarbonate-flux runoff relationships. Differences brought about by the dissimilarities in the lithology distributions are for each of the four fluxes either similar, or smaller by a factor of two to four. Finally, it is interesting to notice that GEM-CO_2* produces with GGHYDRO the couple of total CO_2 consumption and HCO_3^- production rates that compares best and the couple of silicate and carbonate CO_2 consumption rates that compares worst with the observational values from Gaillardet et al. (1999), as quantified by the root mean square difference. The same root mean square difference shows that the GEM-CO_2/GGHYDRO combination produces the set of total HCO_3^- total CO_2, silicate weathering CO_2 and carbonate weathering CO_2 fluxes that is all in all in best agreement with Gaillardet et al. (1999).

3.1.3 Analysis of model-data differences

The large discrepancies between the CO_2 consumption or the HCO_3^- production rates calculated with the two models and the literature values based on river hydrochemistry data (Gaillardet et al., 1999) are more difficult to explain. The consideration of hydrochemistry data from catchments that are not purely monolithologic represents a potential source of uncertainty for the calculated CO_2 consumption rates. Even minor occurrences of carbonate outcrops in silicate catchments can easily lead to substantially overestimated CO_2 consumption rates for silicate mineral dissolution: part of the measured HCO_3^- would in this case be provided by the more readily dissolving carbonate minerals. An equivalent amount of atmospheric CO_2 consumed should accordingly be accounted for in the carbonate weathering CO_2 consumption. Bluth and Kump (1994) discuss this issue in connection with the high denudation rates they observe for shale catchments. Amiotte Suchet and

Probst (1995b) further count sandstones among the problematic rock types. Similarly, but probably less important, carbonate catchments might contain a substantial fraction of slowly-weathering silicate outcrops. In this case, the assumption that half of the measured HCO_3^- in water samples is of atmospheric origin would lead to an underestimation of the actual CO_2 consumption rate in such catchments, and of the pure carbonate weathering rate.

The empirical relationships of Bluth and Kump (1994) used with GKWM are probably more prone to such effects than those of Amiotte Suchet and Probst (1993), used with GEM-CO_2 and GKWM*. Bluth and Kump (1994) considered catchments with basin areas ranging from 1.7 to 27,216 km^2 (median: 342 km^2). The catchments considered by Meybeck (1986), where the hydrochemistry data used by Amiotte Suchet and Probst (1993) come from, are about two orders of magnitude smaller. They cover between 1.15 and 225.1 km^2 (median: 7.8 km^2); the second largest one already covers only 78.7 km^2. It can be expected that the smaller basins respond more strictly to the critical monolithology requirement than the larger ones. On the other hand, the catchments selected by Bluth and Kump (1994) cover a much larger diversity of geographical and climatic conditions than those of Meybeck (1986) and might thus be more representative of the global Earth. The data set used by Bluth and Kump (1994) also presents an incomparably better temporal coverage than that of Meybeck (1986).

However, it is clear that, even if some corrective factor could be introduced into the formulation of GKWM to correct for the relatively high CO_2 consumption rates, HCO_3^- production rates would not be affected and thus remain far too low. Ludwig et al. (1998) address the issue of the low HCO_3^- production rates in GEM-CO_2 by introducing an additional climate dependency. They first integrate GEM-CO_2 HCO_3^- fluxes over the areas covered by thirty-one large river basins. For each of these basins, the total flux is further partitioned into six fractions contributed by six different climatic subunits within the basin. A multiple regression is then used to calculate climatic weights for each of the six classes of fractional contributions so that their weighted sum would fit the observed fluxes for the thirty-one river basins. Only four of the six adjusted weights turn out to be statistically significant. They span a wide range from 0.85 for the tropical wet to 6.55 for temperate dry climatic subunits. Ludwig et al. (1998) find that the modelled global HCO_3^- production increases from 27.5 Tmol/yr to 36.9 Tmol/yr and the global CO_2 consumption from 19.4 Tmol/yr to 26.4 Tmol/yr as a result of the proposed correction. The corrected flux values compare well with the figures from Gaillardet et al. (1999).

The correction proposed by Ludwig et al. (1998) was nevertheless not considered for this study. It was also disregarded by Ludwig et al. (1999). As will be seen below, the variability in the calculated glacial-interglacial flux variations based on runoff ($P - E$) variations alone is already so high that their interpretation will only be impeded by additional climate forcings. Finally, and most importantly, the predictive improvement brought about by the proposed correction is expensive if

the additional requirements are considered. The number of parameters is increased from six to ten. The four extra parameters do also not even have any physical meaning. The distributions of two additional climatic variables (annual average biotemperature and total annual precipitation) are required to determine the distribution of the six climatic subunits. Three climatic forcings are thus required now instead of one. The improved flux values are thus, physically speaking, not necessarily more significant.

A discussion of the performances of the two models would be incomplete without an assessment of the fundamental validity and expected reliability of the empirical approach that the two models are based on. The empirical relationships used in the two models actually derive from log-log correlations of bicarbonate production rates with runoff. The linear relationships from Amiotte Suchet and Probst (1993) are actually also log-log type relationships with a slope of exactly one. Gaillardet et al. (1999) expressed serious concerns regarding the physical sense of log-log correlations of weathering rates with runoff, suggesting even that such correlations do not contain any pertinent information, especially when the slope is close to one. However, as long as no mechanistic model of continental weathering processes exists, the kind of empirical model used here represents the best available *continent-based* option to assess the glacial-interglacial variations of atmospheric CO_2 consumption and river HCO_3^- production rates.

3.2 Glacial-interglacial variations

3.2.1 Runoff variations

The net LGM-minus-present-day variations of the runoff volumes over the three relevant zones (L1, L2, and S1), as derived from each of the eight GCM climate data sets combined with the two runoff distribution data sets are reported in Tables 5 (GKWM landmask) and 6 (GEM-CO_2 landmask). The total net variation represents the difference between the LGM and the present-day water fluxes over the areas respectively exposed at these two periods. It is made up by the net variation over zone L1 increased by the calculated LGM runoff from S1 reduced by the present-day amount of water running off from the regions in L2.

There is clearly no agreement between the estimated runoff variations in the regions exposed both now and at the LGM (zone L1) derived from the eight GCM simulation experiments. The same holds for the total net variations. Even ECHAM3.fix and CCM1.cal, the two model experiments that produced the most realistic present-day global runoff volumes among the eight selected ones, lead to contradicting conclusions. For each zone, CCM1.cal predicts substantially greater variations (i. e., smaller decreases and larger increases) than ECHAM3.fix. Both lead to lower runoff volume over the L1 regions at the LGM, but there are large differences between the

Table 5
LGM-minus-present-day runoff variations for exposed areas on the GKWM landmask (externally drained only).

	GGHYDRO				UNH-GRDC			
	L1	L2	S1	Total net	L1	L2	S1	Total net
BMRC2.fix	−1,300	−7,900	10,100	900	−400	−5,900	7,900	1,600
CCC2.0.fix	−2,800	−7,900	8,700	−2,000	−2,300	−5,900	6,500	−1,700
ECHAM3.fix	−5,100	−7,900	9,000	−4,000	−4,400	−5,900	6,900	−3,400
LMCELMD5.fix	−1,400	−7,900	8,200	−1,100	−800	−5,900	6,400	−300
CCC2.0.cal	1,500	−7,900	8,800	2,400	2,000	−5,900	6,600	2,700
CCM1.cal	−400	−7,900	10,700	2,400	100	−5,900	8,500	2,700
GFDL.cal	−2,800	−7,900	10,700	0	−2,500	−5,900	8,400	0
UKMO.cal	−2,900	−7,900	10,400	−400	−1,900	−5,900	8,200	400
Average	−1,900	−7,900	9,600	−200	−1,300	−5,900	7,400	200

All fluxes are given in km^3/yr and have been rounded to the nearest hundred before reporting. The "Total net" response represents the difference between runoff over areas exposed at the LGM (L1+S1) and those exposed at present (L1+L2).

Table 6
LGM-minus-present-day runoff variations for exposed areas on the GEM-CO_2 landmask (externally drained only).

	GGHYDRO				UNH-GRDC			
	L1	L2	S1	Total net	L1	L2	S1	Total net
BMRC2.fix	−1,300	−7,700	10,100	1,100	−500	−5,700	7,900	1,700
CCC2.0.fix	−3,000	−7,700	8,700	−2,000	−2,500	−5,700	6,500	−1,700
ECHAM3.fix	−5,300	−7,700	9,000	−4,000	−4,600	−5,700	6,900	−3,400
LMCELMD5.fix	−1,900	−7,700	8,200	−1,400	−1,300	−5,700	6,500	−600
CCC2.0.cal	1,200	−7,700	8,700	2,200	1,700	−5,700	6,600	2,500
CCM1.cal	−500	−7,700	10,700	2,500	−100	−5,700	8,500	2,700
GFDL.cal	−2,900	−7,700	10,700	100	−2,500	−5,700	8,300	100
UKMO.cal	−2,900	−7,700	10,400	−200	−2,000	−5,700	8,200	500
Average	−2,100	−7,700	9,600	−200	−1,500	−5,700	7,400	200

See Table 5 for further details.

predicted variations. Regarding the total net variations, the results obtained with these two models are even more contrasting. In the four subsets of runoff variations, the largest total net decrease is each time produced by ECHAM3.fix and the largest net increase by CCM1.cal. Finally, it is interesting to notice that there seems to be a slight tendency for the GCM with fixed SSTs ('.fix' simulations) to produce lower variations (i. e., larger decreases and smaller increases) in each zone than those with calculated SSTs ('.cal' simulations). However, the due to the large scatter in the results, the tendency is not statistically significant.

There are systematic differences between the variations based on either GGHYDRO or UNH-GRDC. On the GKWM landmask, e. g., and with the GGHYDRO runoff distribution, the calculated LGM-minus-present-day variations range between $-5{,}100$ and 1,500 km^3/yr for zone L1 and between 8,200 and 10,700 km^3/yr for zone S1; together with the 7,900 km^3/yr increase in zone L2 they lead to total net variations ranging from a 4,000 km^3/yr reduction to a 2,400 km^3/yr increase. Variations based on UNH-GRDC are 300–1,000 km^3/yr greater in zone L1, 2,000 km^3/yr greater in zone L2, and $1{,}800$–$2{,}300$ km^3/yr lower in S1. The total net variations based on UNH-GRDC are finally either similar or up to 800 km^3/yr greater than those based on GGHYDRO. Similar figures are obtained on the GEM-CO_2 landmask. On the whole, the systematic differences are, however, not significant. In each of the two subsets of estimates, based on either GGHYDRO or UNH-GRDC, the variations in zone L1 cover a range of about 6,200–6,700 km^3/yr. The maximum difference between estimates in the two subsets respectively based on the same GCM results is only 1,000 km^3/yr, more than six times less. Over the exposed shelf (zone S1), each set of variations based on either GGHYDRO and UNH-GRDC cover a range of 2,100–2,600 km^3/yr, which is comparable to the differences between the respective estimates from two subsets. In zone S1 the uncertainties on the calculated variations are thus equally influenced by the variabilities of the "present-day" runoff values (i. e., the values extrapolated from the nearby continents) on one hand and the GCM derived glacial-interglacial anomalies on the other hand.

Using the means of the sixteen individual variations as best estimates, it can be concluded that the global runoff volumes were $1{,}650 \pm 700$ km^3/yr lower at the LGM in the areas exposed both now and then (L1). They were 6,400–7,900 km^3 lower in the areas that got covered by ice (only two actual estimates available), and they were $8{,}500 \pm 500$ km^3/yr over the shelf that got exposed. The global runoff volume was probably the same at the LGM as today, to within ± 800 km^3/yr.

The uncertainties quoted above represent the standard errors of the means in the respective areas and take into account that the sixteen individual estimates are not really independent of each other. They rather come in pairs. There is one pair for each of the eight GCMs. The two values of each pair are based on either GGHYDRO or UNH-GRDC. Considering the sixteen estimates as independent of each other would lead to unrealistically low standard errors of the means. For the rest of this discussion, quoted uncertainties are always standard errors of the correspond-

ing means. Where they relate to the whole set of the sixteen variations, they were calculated from the eight means of the pairs of estimates. Where they relate to one of the two subsets based on either GGHYDRO or UNH-GRDC only, they represent the usual standard error of the mean of that subset. In either case, multiply the quoted uncertainties by the appropriate *Student's t* factors at seven degrees of freedom to derive confidence intervals at any desired confidence level (2.365 for the 95% and 3.499 for the 99% confidence level).

3.2.2 CO_2 consumption and HCO_3^- production rate variations

Global net LGM-minus-present-day variations of CO_2 consumption and HCO_3^- production rates calculated with the two weathering models in conjunction with the sixteen estimates of runoff distribution variations are detailed in Tables 7 (for GKWM) and 8 (for GEM-CO_2). Flux variations for the three zones based on the individual GCM data sets are illustrated in Figure 2, where for clarity reasons, only the pairwise means of variations obtained with each GCM on the basis of GGHYDRO and UNH-GRDC are drawn.

The three zones produce markedly different effects. The mean of the sixteen total HCO_3^- production rate variation obtained with GKWM (Table 7) is 6.2 ± 0.6. It is made up of an absolute variation of -0.7 ± 0.3 Tmol/yr in the areas exposed both now and at the LGM (L1), a decrease of 4.6–5.8 Tmol/yr due to ice cover (L2) and an increase of 12.1 ± 0.5 Tmol/yr due to shelf exposure (S1). With GEM-CO_2 (Table 8) the total mean variation is 9.4 ± 1.0. The three contributions are -0.9 ± 0.6 Tmol/yr (L1), 3.3–4.4 Tmol/yr (L2) and 14.1 ± 0.7 Tmol/yr (S1). The mean global CO_2 consumption rate variation obtained with GKWM is 2.8 ± 0.4 Tmol/yr, made up of an absolute variation of -0.7 ± 0.3 Tmol/yr over zone L1, a 3.7–4.6 Tmol/yr decrease over zone L2 and an increase of 7.7 ± 0.3 Tmol/yr over S1. With GEM-CO_2, the mean global variation is 4.8 ± 0.6 Tmol/yr and the three contributions are -0.8 ± 0.4 Tmol/yr (L1), 2.4–3.1 Tmol/yr (L2) and 8.3 ± 0.4 Tmol/yr (S1).

The increase of HCO_3^- production due to shelf exposure is 2.0–4.4 times as large as the decrease due to the ice cover. For CO_2 consumption, the increase due to shelf exposure is about 1.6–3.6 times as large as the decrease due to the ice cover. The variations in zone L1 are always more than 3.5 times lower than in zone S1. As a consequence, all of the sixty-four calculated sets of flux variations indicate that the total net HCO_3^- and CO_2 fluxes were both higher at the LGM than they are today.

For each GCM $P-E$ distribution, GEM-CO_2 always produces larger increases than GKWM of both HCO_3^- production and CO_2 consumption rates than GKWM in zone S1, and also greater net variations. The decreases of both fluxes in zone L2 are larger with GKWM than with GEM-CO_2. It is difficult to make out a clear picture of the flux variations produced by the two weathering models for zone L1. GCMs

Table 7
GKWM LGM-minus-present-day variations of HCO_3^- and CO_2 fluxes from continental weathering (externally drained areas only).

	GGHYDRO				UNH-GRDC			
	ΔHCO_3^- total	ΔCO_2 total	ΔCO_2 silic.	ΔCO_2 carb.	ΔHCO_3^- total	ΔCO_2 total	ΔCO_2 silic.	ΔCO_2 carb.
BMRC2.fix	8.0	3.9	−0.2	4.1	7.0	3.65	0.3	3.35
CCC2.0.fix	5.0	1.95	−1.1	3.05	4.1	1.65	−0.8	2.45
ECHAM3.fix	4.4	1.25	−1.9	3.15	3.55	1.05	−1.45	2.5
LMCELMD5.fix	4.75	1.75	−1.25	3.0	4.45	1.8	−0.85	2.65
CCC2.0.cal	6.8	3.3	−0.2	3.5	5.9	3.0	0.1	2.9
CCM1.cal	9.0	4.5	0.0	4.5	8.0	4.2	0.4	3.8
GFDL.cal	7.8	3.5	−0.8	4.3	6.55	3.0	−0.55	3.55
UKMO.cal	7.6	3.15	−1.3	4.45	6.7	2.9	−0.9	3.8
Mean	6.65 ± 0.6	2.9 ± 0.4	-0.85 ± 0.2	3.75 ± 0.2	5.75 ± 0.6	2.65 ± 0.4	-0.45 ± 0.2	3.1 ± 0.2

All fluxes are given in 10^{12} mol/yr and were rounded before reporting. The quoted uncertainties for the mean variations are the standard errors of the means ($n = 8$). Multiply them by 2.365 or 3.499 to derive confidence intervals at the 95% and 99% confidence levels respectively (*Student's t* factors for d.f. = 7)

Table 8
GEM-CO_2 LGM-minus-present-day variations of HCO_3^- and CO_2 fluxes from continental weathering (externally drained areas only).

	GGHYDRO				UNH-GRDC			
	ΔHCO_3^- total	ΔCO_2 total	ΔCO_2 silic.	ΔCO_2 carb.	ΔHCO_3^- total	ΔCO_2 total	ΔCO_2 silic.	ΔCO_2 carb.
BMRC2.fix	12.1	6.3	0.5	5.8	10.1	5.3	0.5	4.8
CCC2.0.fix	6.45	2.85	−0.75	3.6	4.7	1.95	−0.8	2.75
ECHAM3.fix	7.3	3.5	−0.3	3.8	5.4	2.55	−0.3	2.85
LMCELMD5.fix	7.3	3.8	0.3	3.5	6.2	3.25	0.3	2.95
CCC2.0.cal	11.1	6.0	0.9	5.1	9.15	5.0	0.85	4.15
CCM1.cal	13.25	7.15	1.05	6.1	11.4	6.2	1.0	5.2
GFDL.cal	12.65	6.5	0.35	6.15	10.4	5.35	0.3	5.05
UKMO.cal	12.3	6.05	−0.2	6.25	10.5	5.2	−0.1	5.3
Mean	10.3 ± 1.0	5.25 ± 0.6	0.2 ± 0.2	5.05 ± 0.4	8.5 ± 0.9	4.35 ± 0.5	0.2 ± 0.2	4.15 ± 0.4

See Table 7 for further details.

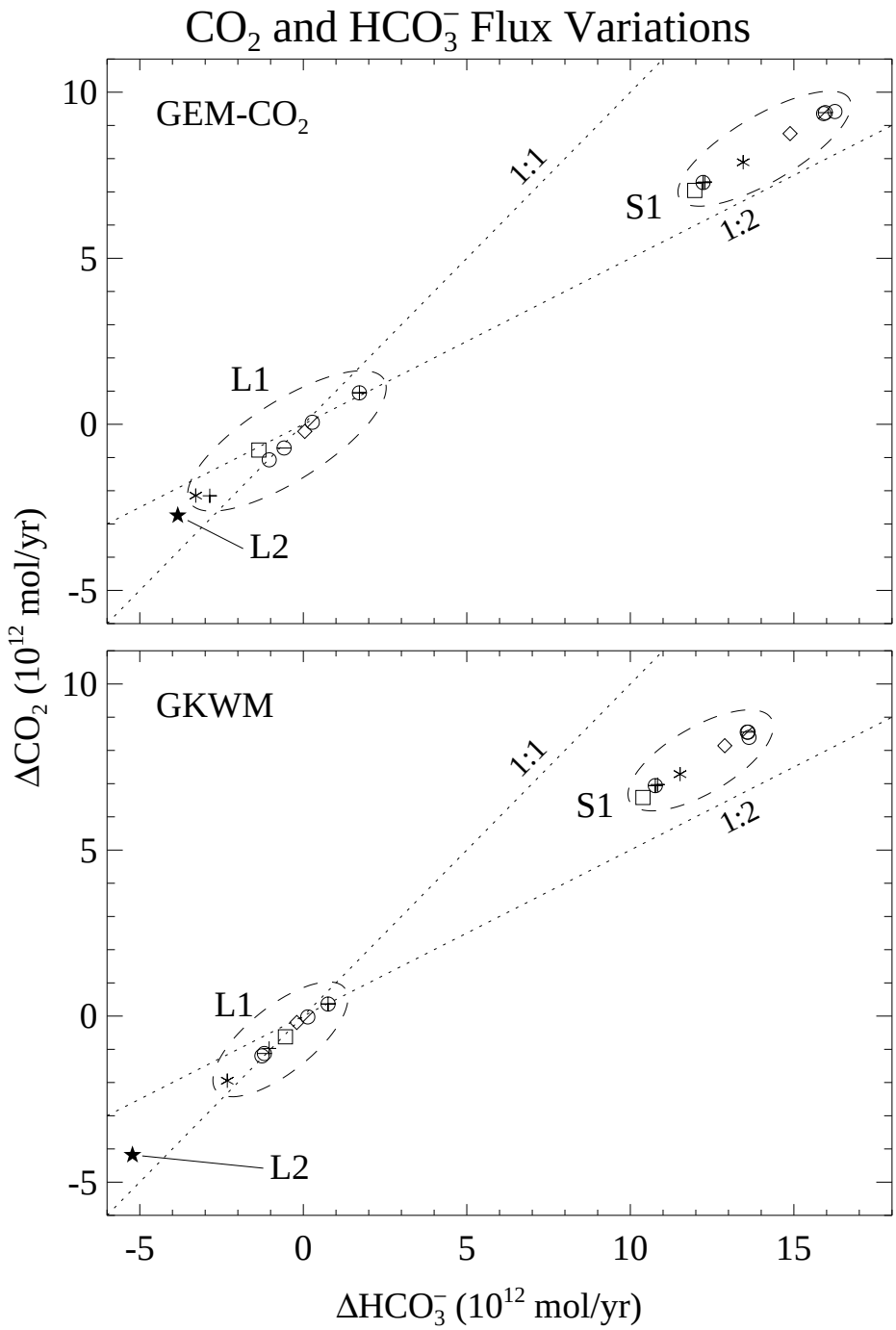

Fig. 2. CO_2 consumption and HCO_3^- production rate variations in zones L1, L2 and S1. Comparison of the average results obtained with GEM-CO_2 and GKWM for each GCM climate data set with the two runoff data sets: ($\diamond$) BMRC2.fix; ($+$) CCC2.fix; ($\oplus$) CCC2.cal; ($\oslash$) CCM1.cal; ($*$) ECHAM3.fix; ($\ominus$) GFDL.cal; ($\square$) LMCELMD5.fix; ($\bigcirc$) UKMO.cal. The dotted lines indicate the ΔCO_2-ΔHCO_3^- combinations that arise from silicate weathering changes alone ($\Delta CO_2 : \Delta HCO_3^- = 1 : 1$) and from carbonate weathering alone ($\Delta CO_2 : \Delta HCO_3^- = 1 : 2$).

with calculated SSTs ('.cal' experiments) appear to produce greater variations with GEM-CO_2 than with GKWM, for both HCO_3^- and CO_2. For GCMs with fixed SSTs (except for BMRC2.fix), it is GKWM that produces the greatest variations. The mean differences between the variations relative to zone S1 and between the global net variations obtained with GKWM and GEM-CO_2 are significantly different from zero, even at the 99.9% significance level. In zone L1, the mean difference is on the other hand statistically not different from zero, not even at the 50% significance level.

The shelf fluxes are not significantly influenced by the degree of refinement in the lihological composition adopted for the 25% of the shelf area for which no information was provided by the map of Gibbs and Kump (1994). Instead of adopting a single, globally constant, composition of 65% carbonates, 27.5% shales and 7.5% sandstones for these points, the composition was also determined as a function of latitude. All eighteen possible subdivisions of the globe into a whole number of equally wide latitude bands on the 1° grid were considered. The standard lithology uses the crudest resolution, with one single 180° wide band; the finest possible one-hundred and eighty 1° wide bands. For each of the eighteen subdivisions, a least squares procedure was used to calculate the areal proportions of the three rock types in the different latitude bands that would come closest to the distribution in the original GKWM. No statistically significant differences between the mean fluxes respectively calculated from the eighteen different latitudinal distributions was found, neither for HCO_3^- nor for any of the CO_2 fluxes.

3.2.3 Silicate and carbonate weathering CO_2 consumption rate variations

GKWM results lead to variations in the CO_2 consumption rate by silicate weathering that range between a 1.8 Tmol/yr reduction and a 0.4 Tmol/yr increase at the LGM relative to the present. The mean variation is -0.7 ± 0.2 Tmol/yr, a statistically significant decrease (at the 99% significance level). Compared to the present-day reference values of 11.7 Tmol CO_2/yr, the two extremes correspond to an 15% reduction and a 3% increase at the LGM respectively; the mean variation is equivalent to a 6% decrease. According to GEM-CO_2, the variation of this rate ranges between a 0.8 Tmol/yr reduction (equal to 7% of the present-day value) and a 1.1 Tmol/yr increase (9%) at the LGM; the mean variation is 0.2 ± 0.2 Tmol/yr (2%). GEM-CO_2 results thus show a slight tendency towards a higher CO_2 consumption rate by silicate weathering at the LGM. The calculated variation is, however, not significantly different from zero. It should, however, be noticed that the mean variation would become 0.4 ± 0.2 Tmol/yr if the extremely negative results based on CCC2.fix were disregarded. This variation would be more in favour of an increase, although it still not excludes a decrease. Regarding carbonate weathering, both models invariably predict higher CO_2 consumption rates at the LGM than at present. The calculated increases represent 20–50% of the present-day reference value of 12.3 Tmol CO_2/yr (20–35% with GKWM, 20–50% with GEM-CO_2). This

increase is mostly due to the large proportion of carbonate outcrops on the emerged shelves.

Although the models were used with identical boundary conditions over the LGM shelf, GEM-CO_2 systematically produces lower silicate weathering CO_2 fluxes over the exposed shelf area than GKWM, and higher carbonate weathering fluxes. GEM-CO_2 attributes a 30% higher flux of CO_2 to carbonate weathering in these areas than GKWM, just as a first order comparison of the two models' empirical relationships would suggest. The differences are statistically significant at the 99.9% level.

3.2.4 Comparison with previous studies

The singlemost important increase in the CO_2 consumption rate by silicate weathering calculated here (1.05 Tmol/yr, equivalent to 9% of the present-day rate) is even less than one tenth of the minimum increase of 10.7 Tmol/yr calculated by Munhoven and François (1996). As mentioned above, recent findings regarding processes not considered in the calculation by Munhoven and François (1996) might substantially affect the results of the Ge/Si inversion procedure, most likely in the direction of a strongly reduced amplitude of the variations.

Ludwig et al. (1999) provide two different estimates for the glacial-interglacial variations of CO_2 consumption and HCO_3^- production rates. They differ by the adopted assumptions regarding the shelf lithology. For the first estimate, the fluxes over the exposed shelf are extrapolated from those calculated for the areas exposed both now and at the LGM. For their second estimate, Ludwig et al. (1999) adopt a pure carbonate cover on the exposed shelf between 30°S and 30°N, and a homogeneous mixture of shale and sandstone outcrops in a ratio of 40:15 elsewhere on the shelf. Ludwig et al. (1999) justify this particular shelf configuration on the basis of the global characteristics of the shelf reconstruction of Gibbs and Kump (1994). They actually perform two different sensitivity tests with pure shale and pure sandstone outcrops at latitudes higher than 30°. The global net response is then obtained by averaging the two flux distributions in the 40:15 ratio.

With their extrapolation procedure Ludwig et al. (1999) find that both fluxes were globally *lower* at the LGM than in the present day, HCO_3^- production by 1.8 Tmol/yr and CO_2 consumption by 1.0 Tmol/yr (figures converted from the authors' original values in Gt C/yr). With their explicit shelf configuration, they find that both fluxes were *higher* at the LGM, HCO_3^- production by 8.9 Tmol/yr and CO_2 consumption by 3.9 Tmol/yr.

To allow a sensible comparison with the results of Ludwig et al. (1999), the calculations based on GEM-CO_2 discussed above were repeated with GCM results from the older ECHAM2 simulation experiments (Lautenschlager and Herterich, 1990; Lautenschlager, 1991) that were used by Ludwig et al. (1999). Furthermore, flux

estimates were also calculated following the rationale of Ludwig et al. (1999), but on the basis of the sixteen runoff distributions produced here, and, in parallel, with those obtained from ECHAM2.

Regarding runoff variations, Ludwig et al. (1999) only report that the exposed shelf area (here zone S1) contributed for 7,100 km^3/yr at the LGM and that the total runoff was 3,500 km^3/yr lower at the LGM than at present. On the GEM-CO_2 landmask used here, ECHAM2 results were found to lead to runoff volumes of $8,200 \pm 900$ km^3/yr on the shelf at the LGM, and a global net LGM-minus-present-day variation of $-1,450 \pm 350$ km^3/yr (means of the GGHYDRO and UNH-GRDC based results plus/minus one half-width of the range — all the results relative to ECHAM2 are reported this way in the following). When the runoff variations over zones L1, L2 and S1 obtained here with ECHAM2 are normalised to the respective surface areas in Ludwig et al. (1999), the total net LGM-minus-present-day variation becomes $-3,000 \pm 550$ km^3/yr and the runoff volume from zone S1 reduces to $7,650 \pm 950$ km^3/yr. The effect of the surface area normalisation illustrates the large flux differences that can simply arise from minor differences between continental masks.

Although this simple normalisation procedure considerably improves the agreement with the figures of Ludwig et al. (1999), there are other possible reasons for the observed differences that cannot be excluded. Ludwig et al. (1999) use an empirical parameterisation to estimate runoff distribution from the GCM climatology. An empirical approach is likely to produce runoff values that differ in an unpredictable way from the GCMs' $P-E$ distributions. However, in a steady-state regime, $P-E$ must match runoff on annual average.

With the standard shelf configuration adopted here and when driven with runoff variation estimates derived from ECHAM2, GEM-CO_2 produces total net HCO_3^- and CO_2 flux variations of 7.4 ± 0.9 Tmol/yr and 3.6 ± 0.4 Tmol/yr respectively (means of the GGHYDRO and UNH-GRDC based results plus/minus one half-width of the range). When the contributions from zones L1, L2 and S1 are scaled to their respective surface areas as in Ludwig et al. (1999), the net variations become 5.9 ± 0.7 Tmol/yr and 2.6 ± 0.3 Tmol/yr respectively.

A first series of tests was based on a simplified version of the extrapolation method used by Ludwig et al. (1999). The differentiation between climate zones was neglected here, as it does not significantly contribute to the results. The fluxes reported by Ludwig et al. (1999) for the LGM shelf change by less than 1% when this differentiation is disregarded. As mentioned above, HCO_3^- and CO_2 fluxes over the exposed shelf are estimated from those calculated for the areas exposed both now and at the LGM with this method. It is hence implicitely assumed that the lithology over the exposed shelf is constant in space and is the same as the average lithology of the continental areas that remained ice-free at the LGM. The principal effect of using this extrapolation method is a reduction of the shelf weathering fluxes by

about 50–60%, compared to the GEM-CO_2 rates shown in Figure 2 (and reported in Table 8). Most of this reduction results from the implicitely assumed smaller proportions of carbonate (14%) and shale outcrops (25%) on the exposed shelf. In the standard shelf lithology adopted here (and also in Gibbs and Kump (1994)), carbonates cover 45% and shales 40% of the exposed area.

The mean total net LGM-minus-present-day variations obtained here with GEM-CO_2 from the sixteen runoff anomaly distributions when using this extrapolation method are 1.1 ± 0.7 Tmol/yr (HCO_3^-) and 0.7 ± 0.5 Tmol/yr (CO_2). Although these ranges do not exclude lower HCO_3^- and CO_2 fluxes at the LGM, they are not as clearly negative as emphasised by Ludwig et al. (1999). The variability of the results is almost completely due to the GCM related runoff distribution estimates. ECHAM2-derived runoff estimates lead to total net HCO_3^- and CO_2 flux decreases of 0.5 ± 0.1 Tmol/yr and 0.4 ± 0.1 Tmol/yr respectively. After normalisation, these decreases become 1.4 ± 0.2 Tmol/yr (HCO_3^-) and 1.1 ± 0.2 Tmol/yr (CO_2). Once again, the simple normalisation procedure considerably eases the apparent initial disagreement with Ludwig et al. (1999), who found decreases of 1.8 Tmol/yr and 1.0 Tmol/yr respectively.

In the second series of tests, the shelf fluxes at the LGM were directly calculated. The exposed shelf was assumed to be completely covered with carbonates between 30°S and 30°N, and with a homogeneous mixture of shale and sandstone outcrops in a ratio of 40:15 everywhere else. As a result of these modified shelf characteristics, the amount of CO_2 consumed by silicate weathering on the shelf at the LGM reduces by about a quarter (from 2.5 ± 0.1 Tmol/yr to 1.8 ± 0.1 Tmol/yr) and the consumption by carbonate weathering increases by about a quarter (from 5.8 ± 0.3 Tmol/yr to 7.4 ± 0.6 Tmol/yr), in comparison with the standard shelf calculations. The resulting total net flux variations of 11.9 ± 1.4 Tmol/yr (HCO_3^-) and 5.7 ± 0.7 Tmol/yr (CO_2) are accordingly higher than those obtained with the standard shelf configuration. The observed differences result to a large extent from the greater proportion of carbonate outcrops on the shelf. The regions between 30°S and 30°N represent 53% of the total shelf area in the reconstruction used here. By construction, it is thus covered by carbonate, shales and sandstones outcrops in areal proportions of 53%, 34% and 13% respectively. With the ECHAM2 runoff distributions, this shelf configuration leads to higher HCO_3^- production and CO_2 consumption rates at the LGM. The total net increases are 10.3 ± 0.8 Tmol/yr (HCO_3^-) and 4.7 ± 0.4 Tmol/yr (CO_2). After surface areal normalisation, these variations reduce to 8.6 ± 0.6 Tmol/yr and 3.6 ± 0.3 Tmol/yr respectively, in good agreement with the increases of 8.9 Tmol/yr (HCO_3^-) and 3.9 Tmol/yr (CO_2) derived from the sensitivity tests of Ludwig et al. (1999).

4 Conclusions

Glacial-interglacial variations of CO_2 consumption and HCO_3^- production rates by continental weathering were investigated with two models of global continental weathering: GKWM (Gibbs and Kump, 1994) and GEM-CO_2 (Amiotte Suchet and Probst, 1993, 1995b). In both models, distributions of CO_2 consumed and HCO_3^- produced by chemical weathering are linked to the distribution of runoff intensity by empirical bicarbonate flux-runoff relationships for the major rock types. The two models have previously been used to examine glacial-interglacial changes of CO_2 consumption and HCO_3 production by continental weathering (Gibbs and Kump, 1994; Ludwig et al., 1999). However, significant differences between the boundary conditions adopted in the two studies make it difficult to compare the results. Here, the components of the two models were compared and adapted as far as possible in order to avoid different responses due to geographical discrepancies, such as different continental outlines, or different ice sheet distributions at the LGM.

In a preliminary intercomparison exercise, the two models were applied with two different data sets for the present-day runoff distribution (Cogley, 1998; Fekete et al., 2000). The HCO_3^- production rates obtained from the two models are typically 20–30% and CO_2 consumption rates 5–20% below the most recent estimates based on observational data (36.3 Tmol/yr for HCO_3^- and 24.0 Tmol/yr for CO_2 (Gaillardet et al., 1999)). Regarding carbonate and silicate weathering, the differences are still larger. For carbonate weathering, all the calculated rates are between 30% and more than 50% too low. GKWM produces silicate weathering CO_2 consumption rates that are 30–50% too high. Only the silicate weathering rate predicted by GEM-CO_2 agrees with the estimates from the literature. It was shown that differences between the empirical HCO_3^-/CO_2 flux-runoff relationships relationships used with the two models account for most of the inter-model differences in the results. The combination of global HCO_3^- production and CO_2 consumption, silicate and carbonate weathering CO_2 consumption rates calculated with GEM-CO_2 and Cogley's (1998) GGHYDRO runoff distribution was found to agree best with the fluxes derived from the observation.

For the application of the two weathering models under LGM conditions, a revised representation for the shelf areas exposed at the LGM was reconstructed. This shelf configuration was used with both weathering models. Publicly available results data sets from eight different GCM simulation experiments carried out in the framework of the Paleo Modelling Intercomparison Project (PMIP, Joussaume and Taylor, 1995, 2000) were used to produce estimates of LGM-minus-present-day variations in the distribution of continental runoff. These eight anomaly distributions were combined with the two present-day runoff distributions to produce a spectrum of sixteen estimates for the LGM runoff distribution. This variety of estimates helped to provide new quantitative insight into the weathering flux variations derived from GKWM and GEM-CO_2.

The calculated estimates of the total net glacial-interglacial runoff variations cover the extreme range from a 4,000 km^3/yr lower to a 2,700 km^3/yr higher drainage volume at the LGM. However, the mean variation of 0 ± 800 km^3/yr points out that the global drainage volume was most probably not significantly different at the LGM than at present.

The large variability of the calculated LGM runoff volumes is reflected in the estimates of HCO_3^- and CO_2 flux variations. According to GKWM, the global HCO_3^- production rate by continental weathering was 6.2 ± 0.6 Tmol/yr and the global CO_2 consumption rate 2.8 ± 0.4 Tmol/yr higher at the LGM than at present. GEM-CO_2 produced somewhat greater variations of 9.4 ± 1.0 Tmol/yr (HCO_3^-) and 4.8 ± 0.6 Tmol/yr (CO_2). Discrepancies between the results obtained here and those of Ludwig et al. (1999) were examined in two series of additional calculations. The largest part of the observed discrepancies could invariably be attributed to the different methods and model configurations (e.g., continental outlines, shelf extent and lithology, internal drainage pattern) adopted in the two studies.

The respective importances of HCO_3^- and CO_2 flux reductions due to the ice cover, increases due to shelf exposure, and variations in areas exposed both now and at the LGM were determined. For HCO_3^- production, the increase due to extended shelf exposure at the LGM was typically 2.0–4.4 times as large as the decrease due to the ice cover. For CO_2 consumption, this factor was 1.6–3.6. In absolute value, the variations of the two fluxes over the regions exposed now and at the LGM were always more than 3.5 times lower than the increases over the shelf.

The model results were also analysed in terms of CO_2 consumed by silicate and carbonate weathering. According to GKWM, the rate of CO_2 consumption by silicate weathering was between 0.7 ± 0.2 Tmol/yr lower at the LGM than in the present day; the rate of CO_2 consumption by carbonate weathering was 3.4 ± 0.2 Tmol/yr higher. GEM-CO_2 results indicate that silicate weathering consumed 0.2 ± 0.2 Tmol/yr more and carbonate weathering 4.6 ± 0.4 Tmol/yr more CO_2 at the LGM than at present.

It is difficult to single out one or two ‘best’ estimates among the sixty-four sets. One might favour the combination of GEM-CO_2 and GGHYDRO, which produced the present-day HCO_3^- and CO_2 fluxes that came closest to the observations, with ECHAM3.fix or CCM1.cal, the two GCM data sets that produced the most realistic global runoff volumes for the present day. The results obtained from these two combinations range, however, respectively at the lower and upper end of the response spectrum. With ECHAM3.fix, it was found that silicate weathering consumed 0.3 Tmol less (-3%) and carbonate weathering 3.8 Tmol more ($+31\%$) CO_2 each year at the LGM than at present; with CCM1.cal, both types of weathering consumed more CO_2 at the LGM, silicate weathering 1.05 Tmol/yr ($+9\%$) and carbonate weathering 6.1 Tmol/yr ($+50\%$).

The large variability that affects the calculated rates of CO_2 consumption by silicate and carbonate weathering still prevents any truly firm conclusion regarding the actual impact of changing weathering processes on glacial-interglacial atmospheric CO_2 to be drawn. As long as no global process-based model of continental weathering is available, the two empirical models used here represent the best continent-oriented option to reconstruct glacial-interglacial variations of CO_2 consumption and HCO_3^- production rates. However, both models require further development in order to understand and resolve the large discrepancies observed here between the flux distributions they produce and independent ones from the literature.

A first-order estimation based on results obtained with the carbon cycle model of Munhoven and François (1996), indicate that the mean weathering flux variation obtained here with GKWM would lead to an atmospheric p_{CO_2} reduction of 5.7 ± 1.3 ppmv at the LGM. The weathering flux changes calculated with GEM-CO_2 would contribute to reduce atmospheric p_{CO_2} by 12.1 ± 1.7 ppmv at the LGM. With the two potential best-estimate variations reported above, atmospheric p_{CO_2} would be reduced by either 7.9 (ECHAM3.fix) or 19.2 ppmv (CCM1.cal), all oceanic and sedimentary feedbacks being taken into account. This variations would represent respectively 11% and 26% of the total observed $\sim$ 75 ppmv decrease.

Acknowledgements

Thanks are due to P. Amiotte Suchet, C. G. Cogley, B. Fekete, M. Lautenschlager, W. Peltier and their colleagues, and all the PMIP participants for making the results of their research efforts publicly available in numerical form. Insightful reviews by W. Ludwig and L. R. Kump are gratefully acknowledged. Financial support for this work was provided by the U. K. National Environment Research Council through grant GR3/11080. G. M. is a Research Associate with the Belgian National Fund for Scientific Research (F.N.R.S.).

References

Amiotte Suchet, P., 1995. Cycle du carbone, érosion chimique des continents et transferts vers les océans. Sci. Géol. Mém. 97, Institut de Géologie, Université Louis Pasteur, Strasbourg, (In French.).

Amiotte Suchet, P., Probst, J.-L., 1993. Flux de CO_2 consommé par altération chimique continentale: Influences du drainage et de la lithologie. C. R. Acad. Sci. Paris Ser. II 317, 615–622, (In French, with English Abstract.).

Amiotte Suchet, P., Probst, J.-L., 5 1995a. A global 1 degree by 1 degree distribution of atmospheric/soil CO_2 consumption by continental weathering and of riverine HCO_3 yield. Data base DB1012, Carbon Dioxide Information Analy-

sis Center (CDIAC), Oak Ridge, TN, archived at http://cdiac.esd.ornl.gov/ndps/db1012.html.

Amiotte Suchet, P., Probst, J.-L., 1995b. A global model for present-day atmospheric/soil CO_2 consumption by chemical erosion of continental rocks (GEM-CO_2). Tellus 47B (1/2), 273–280.

Barnola, J.-M., Raynaud, D., Korotkevich, Y. S., Lorius, C., 1987. Vostok ice core provides 160,000-year record of atmospheric CO_2. Nature 329, 408–414.

Bluth, G. J. S., Kump, L. R., 1994. Lithologic and climatologic controls of river chemistry. Geochim. Cosmochim. Acta 58 (10), 2341–2359.

Broccoli, A. J., Manabe, S., 1992. The effects of orography on midlatitude Northern Hemisphere dry climates. J. Climate 5, 1181–1201.

Broecker, W. S., 1982. Ocean chemistry during glacial times. Geochim. Cosmochim. Acta 46, 1689–1705.

Broecker, W. S., Peng, T.-H., 1982. Tracers in the Sea. Lamont-Doherty Geological Observatory of Columbia University, Palisades, NY 10964.

Broecker, W. S., Peng, T.-H., 1987. The role of $CaCO_3$ compensation in the glacial to interglacial atmosphere CO_2 change. Global Biogeochem. Cycles 1 (1), 15–29.

Chappell, J., Shackleton, N. J., 1986. Oxygen isotopes and sea level. Nature 324, 137–140.

CLIMAP Project Members, 1981. Seasonal reconstruction of the earth's surface at the last glacial maximum. Geol. Soc. America Map Chart Ser. MC-36.

Cogley, J. G., 1998. GGHYDRO - Global Hydrographic Data, Release 2.2. Trent Climate Note 98-1, Trent University, Dept. of Geography, Peterborough, Ontario.

Colman, R. A., McAvaney, B. J., 1995. Sensitivity of the climate response of an atmospheric general circulation model to changes in convective parameterization and horizontal resolution. J. Geophys. Res. 100, 3155–3172.

Delmas, R. J., Ascencio, J.-M., Legrand, M., 1980. Polar ice evidence that atmospheric CO_2 20,000 yr BP was 50% of present. Nature 284, 155–157.

ETOPO5, 1988. Digital relief of the surface of the earth. Data Announcement 88-MGG-02, NOAA/NGDC, Boulder, CO, archived at ftp://ncardata.ucar.edu/datasets/ds759.1.

Fairbanks, R. G., 1989. A 17,000-year glacio-eustatic sea level record: Influence of glacial melting rates on the Younger Dryas event and the deep-ocean circulation. Nature 342, 637–642.

Fekete, B. M., Vörösmarty, C. J., Grabs, W., 2000. Global composite runoff fields based on observed river discharge and simluated water balances. GRDC Report 22, Global Runoff Data Centre, Bundesanstalt für Gewässerkunde, Koblenz (Germany).

Froelich, P. N., Blanc, V., Mortlock, R. A., Chillrud, S. N., Dunstan, W., Udomkit, A., Peng, T.-H., 1992. River fluxes of dissolved silica to the ocean were higher during glacials: Ge/Si in diatoms, rivers, and oceans. Paleoceanography 7 (6), 739–767.

Gaillardet, J., Dupré, B., Louvat, P., Allègre, C. J., 1999. Global silicate weathering and CO_2 consumption rates deduced from the chemistry of large rivers. Chem.

Geol. 159, 3–30.
Gibbs, M. T., Kump, L. R., 1994. Global chemical erosion during the last glacial maximum and the present: Sensitivity to changes in lithology and hydrology. Paleoceanography 9 (4), 529–543.
Hammond, D. E., McManus, J., Berelson, W. M., Meredith, C., Klinkhammer, G. P., Coale, K. H., 2000. Diagenetic fractionation of Ge and Si in reducing sediments: the missing Ge sink and a possible mechanism to cause glacial/interglacial variations in oceanic Ge/Si. Geochim. Cosmochim. Acta 64 (14), 2453–2465.
Hewitt, C. D., Mitchell, J. F. B., 1997. Radiative forcing and response of a GCM to ice age boundary conditions: cloud feedback and climate sensitivity. Climate Dyn. 13, 821–834.
Jones, I. W., Munhoven, G., Tranter, M., 1999. Comparative fluxes of HCO_3^- and Si from glaciated and non-glaciated terrain during the last deglaciation. In: Tranter, M., Armstrong, R., Brun, E., Jones, G., Sharp, M., Williams, M. (Eds.), Interactions Between the Cryosphere, Climate and Greenhouse Gases. Vol. 256 of Series of Proceedings and Reports. IAHS, Wallingford, pp. 267–272.
Joussaume, S., Taylor, K., 1995. Status of the Paleoclimate Modeling Intercomparison Project (PMIP). In: Gates, W. L. (Ed.), Proceedings of the First International Atmospheric Model Intercomparison Project (AMIP) Scientific Conference. No. 732 in WMO TD. JPS (WCRP/WMO), Geneva, pp. 425–430, (Available online at URL http://www-pcmdi.llnl/pmip/overview.html.).
Joussaume, S., Taylor, K., 2000. The Paleoclimate Modeling Intercomparison Project. In: Braconnot, P. (Ed.), Paleoclimate Modeling Intercomparison Project (PMIP). No. 1007 in WMO/TD. WMO, Geneva (CH), pp. 9–24, (WCRP-111).
Jouzel, J., Barkov, N. I., Barnola, J. M., Bender, M., Chappellaz, J., Genthon, C., Kotlyakov, V. M., Lipenkov, V., Lorius, C., Petit, J.-R., Raynaud, D., Raisbeck, G., Ritz, C., Sowers, T., Stievenard, M., Yiou, F., Yiou, P., 1993. Extending the Vostok ice-core record of palaeoclimate to the penultimate glacial period. Nature 364, 407–412.
King, S. L., Froelich, P. N., Jahnke, R. A., 2000. Early diagenesis of germanium in sediments of the Antarctic South Atlantic: In search of the missing Ge sink. Geochim. Cosmochim. Acta 64 (8), 1375–1390.
Korzoun, V. I., Sokolov, A. A., Budyko, M. I., Voskresensky, K. P., Kalinin, G. P., Konoplyantsev, A. A., Korotkevich, E. S., Lvovich, M. I., 1977. Atlas of World Water Balance. The UNESCO Press, Paris.
Kump, L. R., Alley, R. B., 1994. Global chemical weathering on glacial time scales. In: National Research Council, Panel on Global Surficial Geofluxes (Ed.), Material Fluxes on the Surface of the Earth. National Academy Press, Washington DC, pp. 46–60.
Kurtz, A. D., Derry, L. A., 1998. Dust-driven glacial/interglacial variations in marine dissolved silica fluxes: Evidence from Ge/Si. EOS Trans. AGU 79 (Fall Meet. Suppl.), F426.
Kutzbach, J. E., Gallimore, R., Harrison, S., Behling, P., Selin, R., Laarif, F., 1998. Climate and biome simulations for the past 21,000 years. Quat. Sci. Rev. 17 (6/7),

473–506.
Lautenschlager, M., 1991. Simulation of the ice age atmosphere – January and July means –. Geol. Rundsch. 80 (3), 513–534.
Lautenschlager, M., Herterich, K., 1990. Atmospheric response to ice age conditions: Climatology near the Earth's surface. J. Geophys. Res. 95 (D13), 22547–22557.
Legates, D. R., Willmott, C. J., 1990. Mean seasonal and spatial variability in global surface air temperature. Theor. Appl. Climatol. 41, 11–21.
Lorenz, S., Grieger, B., Helbig, P., Herterich, K., 1996. Investigating the sensitivity of the Atmospheric General Circulation Model ECHAM 3 to paleoclimatic boundary conditions. Geol. Rundsch. 85, 513–524.
Ludwig, W., Amiotte-Suchet, P., Munhoven, G., Probst, J.-L., 1998. Atmospheric CO_2 consumption by continental erosion: present-day controls and implications for the last glacial maximum. Global Planet. Change 16-17 (1-4), 107–120.
Ludwig, W., Amiotte-Suchet, P., Probst, J.-L., 1999. Enhanced chemical weathering of rocks during the last glacial maximum: a sink for atmospheric CO_2 ? Chem. Geol. 159 (1-4), 147–161.
Masson, V., Joussaume, S., Pinot, S., Ramstein, G., 1998. Impact of parameterizations on simulted winter mid-Holocene and Last Glacial Maximum climatic changes in the northern hemisphere. J. Geophys. Res. 103 (D8), 8935–8946.
McFarlane, N. A., Boer, G. J., Blanchet, J.-P., Lazare, M., 1992. The Canadian Climate Centre second-generation General Circulation Model and its equiliubrium climate. J. Climate 5, 1013–1044.
Meybeck, M., 1986. Composition chimique des ruisseaux non pollués de France. Sci. Géol. Bull. 39 (1), 3–77, (In French, with English Abstract.).
Meybeck, M., 1987. Global chemical weathering of surficial rocks estimated from river dissolved loads. Am. J. Sci. 287, 401–428.
Munhoven, G., 11 1997. Modelling glacial-interglacial atmospheric CO_2 variations: The role of continental weathering. Ph.D. thesis, Université de Liège, Liège.
Munhoven, G., 1999. Carbon dioxide consumption and bicarbonate production rates by continental weathering at the LGM and at present-day — an update. In: Tranter, M., Armstrong, R., Brun, E., Jones, G., Sharp, M., Williams, M. (Eds.), Interactions Between the Cryosphere, Climate and Greenhouse Gases. Vol. 256 of Series of Proceedings and Reports. IAHS Press, Wallingford, pp. 273–281.
Munhoven, G., François, L. M., 1996. Glacial-interglacial variability of atmospheric CO_2 due to changing continental silicate rock weathering: A model study. J. Geophys. Res. 101 (D16), 21423–21437.
Neftel, A., Oeschger, H., Schwander, J., Stauffer, B., Zumbrunn, R., 1982. Ice core samplements give atmospheric CO_2 content during the past 40,000 yr. Nature 295, 220–223.
Peltier, W. R., 1994. Ice age paleotopography. Science 265, 195–201.
Petit, J.-R., Jouzel, J., Raynaud, D., Barkov, N. I., Barnola, J.-M., Basile, I., Bender, M., Chappellaz, J., Davis, M., Delaygue, G., Delmotte, M., Kotlyakov, V. M., Legrand, M., Lipenkov, V. Y., Lorius, C., Pépin, L., Ritz, C., Saltzman, E., Stieve-

nard, M., 1999. Climate and atmospheric history of the past 420,000 years from the Vostok ice core, Antarctica. Nature 399, 429–436.

White, A. F., Bullen, T. D., Vivit, D. V., Schulz, M. S., Clow, D. W., 1999. The role of disseminated calcite in the chemical weathering of granitoid rocks. Geochim. Cosmochim. Acta 63 (13-14), 1939–1953.

Willmott, C. J., Rowe, C. M., Mintz, Y., 1985. Climatology of the terrestrial seasonal water cycle. J. Climatol. 5, 589–606.